

Journal of Basics and Applied Sciences Research (JOBASR) ISSN (print): 3026-9091, ISSN (online): 1597-9962

Volume 1(1) IPSCFUDMA 2025 Special Issue DOI: https://dx.doi.org/10.4314/jobasr.v1i1.1s



Mapping of Conductive Zones for Groundwater Potential Using VLF-EM Method in Akwanga, Nasarawa State Nigeria

Ubaidullah, A.1*, Aisha A. K.2, Ayyaninuola O. S.3 & Tukur R. S.3

- ¹Department of Geophysics, Federal University Dutsin-Ma, Katsina State.
- ²Department of Geology, Nasarawa State University Keffi, Nasarawa State.
- ³Department of Physics, Nasarawa State University Keffi, Nasarawa State.
- *Corresponding Author Email: uahmad22@fudutsinma.edu.ng



ABSTRACT

Very low frequency (VLF) electromagnetic measurements were carried out in Akwanga for the mapping of fractured and conductive zoneswith the aim of delineating subsurface structures associated with groundwater occurrence by determining the depth and lateral extent of conductive zones inferred as major aguifers in the study area. A total of twelve (12) profiles were carried out with 10m sample interval along each profile and spread length ranging between 120m and 560m using GEM-19 VLF System. The field data obtained were processed, filtered and interpreted using Karous-Hjelt (K-H) filtered pseudo-section to visualise 2-D conductivity image of the subsurface. The results of the study showed the presence of fracture zones and are prominently oriented in the NE-SW and NW-SE direction. The result also revealed that most of the fractured zones were located at a depth range of 0 up to 60m within the subsurface. The presence of and interconnectivity of the fracture zones show that the study area has good prospects for groundwater. On the basis of the investigation The study therefore recommends the drilling of productive and sustainable boreholes at locations traverse 1, traverse 2, traverse 4, traverse 6, traverse 7 and traverse 10between 150-250 m, 75-175 m, 150-200 m, 120-220 m, 250-300 m and 160-220 m respectively along the profile.

Keywords:

electromagnetic method, fractured zones, groundwater, traverse, very low frequency (VLF)

INTRODUCTION

Ground water is a vital resources and it supports human existence on earth, therefore its quantity is extremely important with regards to domestic consumption, water supply for industry and agriculture (Nura *et al.*, 2019). Groundwater is an outstanding source of water as it is renewable and usually of greater quality than surface water (Aisha *et al.*, 2022). It is readily available throughout the year and it is cheaper to access than exploring for and exploiting surface water, it is more portable and not easily contaminated as surface water (Ahzegbobor, 2010)

Akwanga is a densely populated area and the vast majority Akwanga inhabitants, inrespective of social status, rely on hand-dug wells and bore-holes for their daily water demands. Considering the growing population, increased agricultural activities within the study area, it is therefore very important to be informed about the quantity of groundwater supply for various purposes in the study area.

The very low frequency electromagnetic (VLF-EM) method has been widely used in the exploration of

conductive near surface features, such as water filled fracture zones. Fracture zones are of great importance in many fields, they are often filled with groundwater, making them conductive bodies measureable with a VLF instrument. The approach uses signal emission from military navigation radio transmitters. There are roughly 42 global ground military communication transmitters that operate in the VLF range of 15-30 kHz. They produce effective signals that can be utilized for a variety of applications such as navigation and communication, groundwater detection and environmental problems, as well as groundwater studies. The detected VLF-EM anomalies usually are interpreted using anomaly curves and monograms (Kaikkonnen and Sharma, 1997; Saaty, 1980). Fraser and Hjelt filtering, followed by contouring of the observed responses, are the most popular procedures to generate qualitative information about the subsurface (Fraser, 1969; Karous and Hjelt 1983).

Akwanga town is plagued with known water challenge and failed boreholes hence this study is motivated by a desire to investigate the groundwater potential in Akwanga town using a time-domain Very Low Frequency (VLF) electromagnetic method. This is necessary because the residents of the study area rely largely on groundwater for their needs.

The Study Area

The research geographical area is the Akwanga local

government in Nasarawa state, North-Central Nigeria (Figure 1). It is located within longitudes 8°18′E and 8°54′E of the Greenwich Meridian and latitudes 8°15′N and 9°20′N of the Equator. The study area is accessible through a network of roads along Keffi-Lafia Express Way.

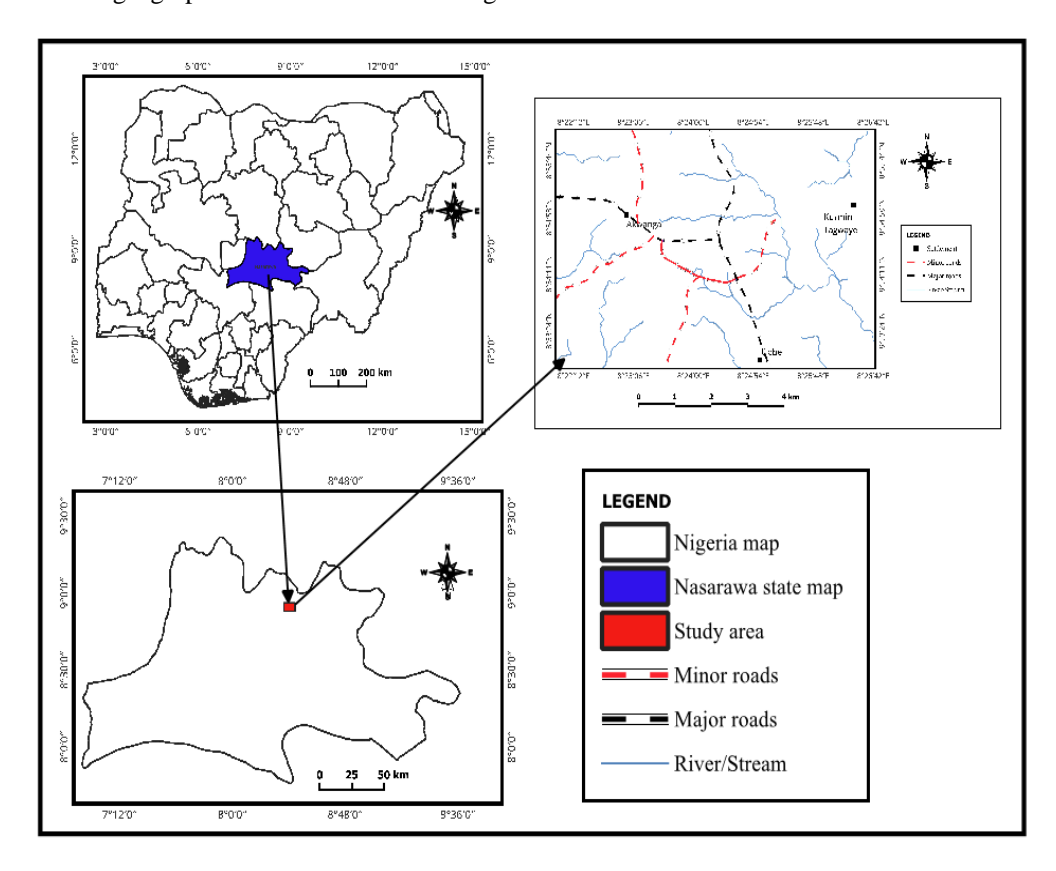


Figure 1: Location Map of the Study Area

Geology of the Study Area

The study area is situated within the basement complex of the north-central Nigeria, The Precambrian Basement Complex rocks of Nigeria outcropping in North central Nigeria show predominant structural trends of N-S to NE-SW but remnant of E-W and NW-SE also exist (Ayanninuola *et al.*, 2018). It consists of various rock units with the predominant including granitic-gneiss, muscovite-schist and migmatite-gneiss (Figure 3) which mostly occur as vein and not mapable (Jatau *et al.*, 2020). The granite gneiss in the research area is light grey and medium grained, consisting of plageoclase, quartz,

microcline, muscovite, and biotite. The exposed rocks are typically low-lying and have numerous joints as a result of both biological and physical degradation. The muscovite-schist is dark grey with very fine-grained texture, composed of quartz, plagioclase-fieldspar, and biotite. The migmatite-gneiss is coarse-grained, white to pinkish, and consists of quartz, feldspar (potassium feldspar and plagioclase), and mica (biotite and muscovite), and occurs as late intrusive members (veins and dykes) in the rock exposure orientated NW-SE, with a thickness of about 2 cm -1.5 cm.

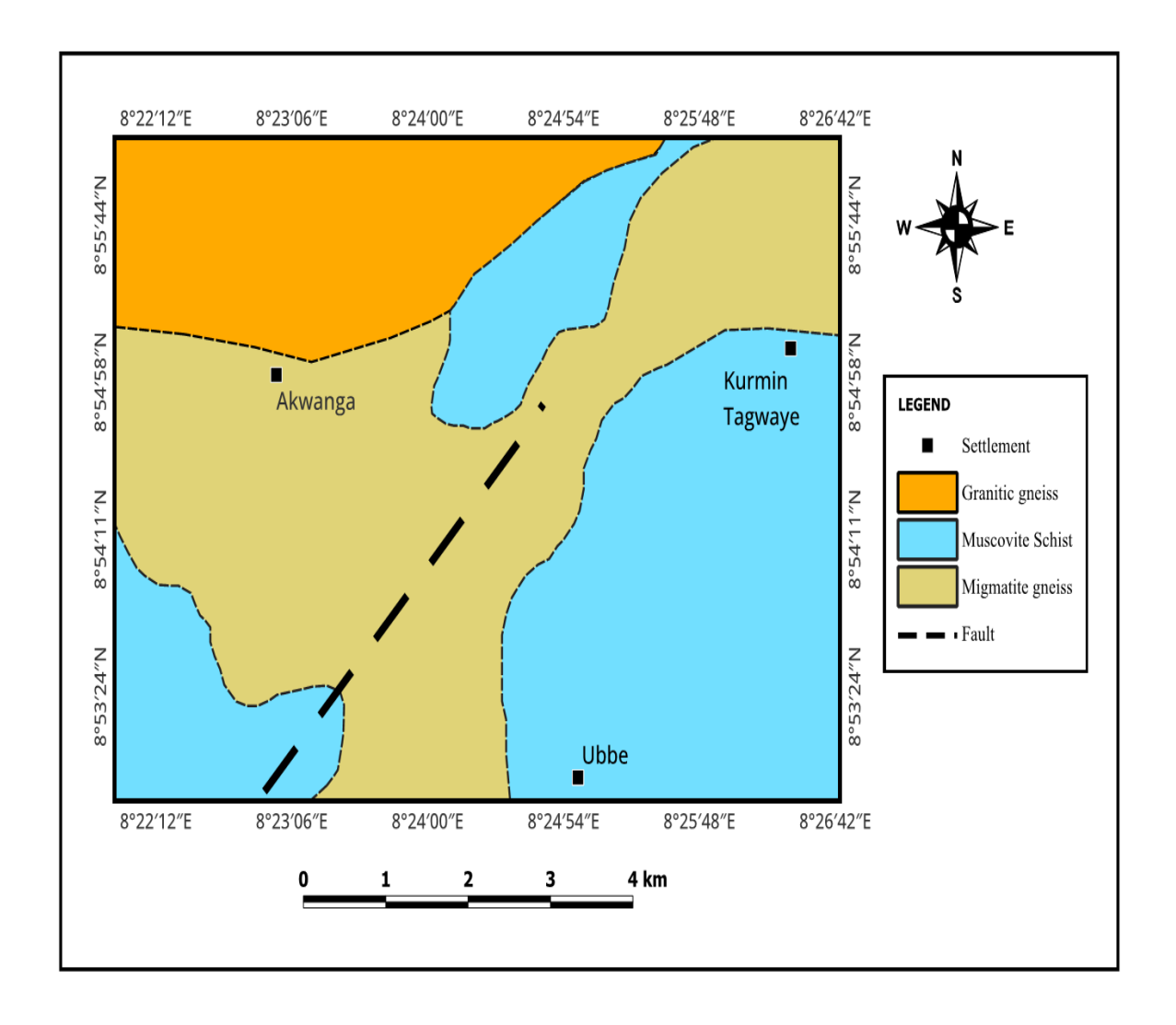


Figure 3: Gelogical Map of the Study Area

Theory

Electromagnetic Method

The electromagnetic field begins with Maxwell's equation, which may be expressed in terms of four vector functions: the electrical field (E), dielectric displacement (D), magnetic field intensity (H), and magnetic induction (B). The four equations directing the propagation of electromagnetic waves can be obtained from Maxwell's equation, which relate the electric and magnetic field vectors shown below (Equation 1, 2, 3 and 4).

Gauss Law:
$$\nabla \cdot E = \frac{\rho}{\varepsilon_0}$$
 (1)

Magnetic monopoles:
$$\nabla \cdot B = 0$$
 (2)

Faraday's Law:
$$\nabla \times \mathbf{E} = -\frac{\partial \mathbf{B}}{\partial t}$$
 (3)
Ampere's Law: $\nabla \times H = J + \frac{\partial D}{\partial t}$ (4)

Ampere's Law:
$$\nabla \times H = J + \frac{\partial D}{\partial t}$$
 (4)

Subsidiary Equations and Wave Equations

The electromagnetic wave equation can be derived utilising the subsidiary equations listed below as well as

the four Maxwell equations.

$$D = \epsilon E \tag{5}$$

$$B = \mu H \tag{6}$$

$$J = \sigma E \tag{7}$$

where

J represents electrical current density in A/m², q is the electric charge in Coulomb/m³, whereas ε is the electrical permittivity and μ denotes magnetic permeability, σ equals electrical conductivity.

For the propagation of magnetic and electric fields, two electromagnetic wave equations shall be deduced from the maxwells equation and the subsidiary equations

Taking the curl of equation 1 and 2 will give the electromagnetic wave equation for propagation of magnetic field vectors below

$$\nabla^2 E - \varepsilon_0 \frac{\delta^2 E}{\delta t^2} - \mu_0 \sigma \frac{\delta E}{\delta t} = 0$$
 (8)

$$\nabla^2 H - \varepsilon_0 \mu_0 \frac{\delta^2 H}{\delta t^2} - \mu_0 \sigma \frac{\delta H}{\delta t} = 0 \tag{9}$$

Equations 8 and 9 regulate the electromagnetic field in a homogeneous, linear media with a charge density of zero, whether the medium is conductive or non-conductive.

Hence considering the angular frequency of low electromagnetic fields

$$w = 2\pi f \tag{10}$$

$$\varepsilon(t) = \varepsilon_0 e^{i\omega t} \tag{11}$$

$$H(t) = H_0 e^{i\omega t} \tag{12}$$

If it is sinusoidal (time varying), substituting equation 11 and 12 into 8 and 9 yields

$$\nabla^2 E - \varepsilon_0 \mu_0 i w^2 E - \mu_0 \sigma i w^2 E = 0 \tag{13}$$

$$\nabla^2 H - \varepsilon_0 \mu_0 i w^2 H - \mu_0 \sigma i w^2 H = 0 \tag{14}$$

The equations above provide the electromagnetic equation for the propagation of electric and magnetic field vectors in an isotropic, homogeneous medium with conductivity, permeability, and permittivity.

MATERIALS AND METHODS

Materials

- i. GEM-19 VLF System (Figure 4)
- ii. GlobalPositioningSystem (GPS)
- iii. Penanddata sheet



Figure 4: GEM-19VLF System.

Field procedure

The VLF method is an inductive exploration technique that is primarily used to map shallow subsurface structural features in which the primary EM wave induces current flow (Singha, 1990; Kaikkonnen and Sharma, 1997). In principle, it utilises transmitters operating between 15 and 30 kHz as the primary EM wave source. The EM waves propagating into the ground from the source (Hp) induce electriccurrents in any subsurface conductor in their path. The induced current produces a secondary EM field (Hs). The vector sum of the primary field (Hp) and secondary field (Hs) produces the elliptically polarised field over time. These elliptically polarised fields consist of two components of the same frequency, but of different

amplitudes and out of phase with each other. The amplitude of the component that is in phase with the primary field Hp is the tilt angle, while the component that is out of phase with the primary field is the ellipticity.

A total of twelve (12) traverses were established in the N–E directions, with a varying traverse lengths and a regular station intervals of 10 m. In order to prevent errors, the antenna unit was kept vertical for the twelve (12) VLF traverses that were conducted in the study region. A convenient frequency of 15.1 KHz was chosen automatically during the scanning procedure. Additionally, the traversal direction remained constant. The karous-hjelt filter program was used to analyse the raw and filtered data of the secondary field's real and imaginary components after they were acquired.

Data presentation

The raw real and filtered real components of the VLF-EM anomalies were considered and filtered using a Karous–Hjelt (K–H) filter, processed and presented as profiles (Figure 5-16) by plotting the filtered real and imaginary components against distance using Microsoft Excel package, also the corresponding K–H pseudo-sections of the profiles were shown respectively (Figure 5-16). The K–H filter computes the approximate subsurface current density, giving rise to a given profile of the data, and the values are relative across the profile. The output of the K–H filter is relative current density versus surface position at a chosen depth. Lower values of relative current density correspond to higher values of resistivity.

Data interpretation

VLF-EM interpretation is generally quantitative in nature. The real components of the VLF-EM data were transformed to filtered real data (Karous & Hjelt, 1983). Anomalous areas were identified and gross cauterisation was applied to the anomalies. Although both the real and quadrature components of the VLF-EM were measured, the real component data, which are usually more diagnostic of linear features, were processed for qualitative interpretation. The real and imaginary components of the EM fields measured (VLF data), were subjected to Fraser filtering (fraser, 1969)to increase the signal-to-noise ratio of the dataset and enhance the anomaly signature. This filter was applied to the real component of the VLF data to transform the dataset to the filtered real VLF data (Karous & Hjelt, 1983). The filtered real data transform every genuine crossover or inflection point of the real anomaly to positive peaks, while reverse crossover becomes negative peak. The linear features with positive filtered real amplitude (high) in all the profiles show areas with conductivity. The visual inspection of these anomaly curves enabled the

qualitative identification of the top of linear features as points of coincidence of crossover and positive peaks of the real and filtered real anomaly curves (Adiat & Ayuk, 2009).

RESULTS AND DISCUSSION

Interpretation is done by considering the high-amplitude signals, which is diagnostic of weathered or fractured zones. The double plots of the filtered real and filtered imaginary components enable qualitative identification of the top of linear features, i.e. points of coincidence of crossovers and positive peaks of the real and filtered anomalies. Below is the VLF-EM anomaly curves (real component and the filtered real component) along transverses 1–12 (Figure 5-16)

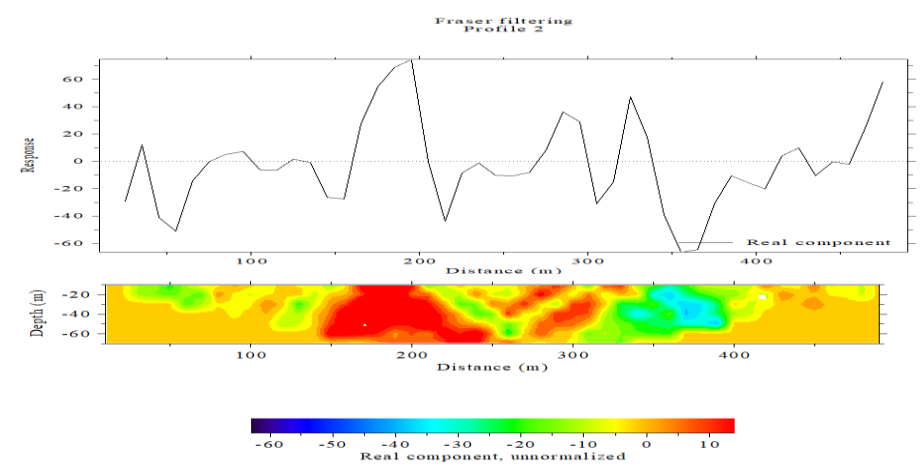


Figure 5: The VLF anomaly plot of in-phase fraser Filtered data and karouse-Hjelt Pseudo cross - section along traverse 1.

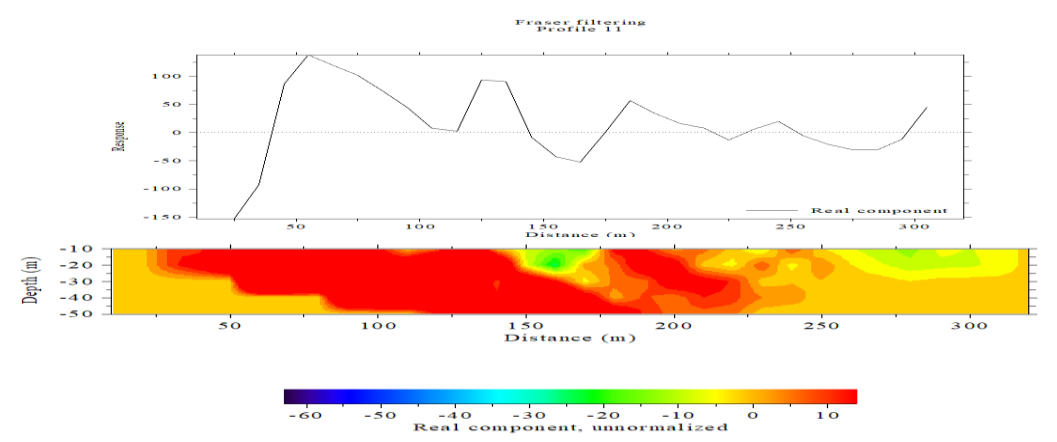
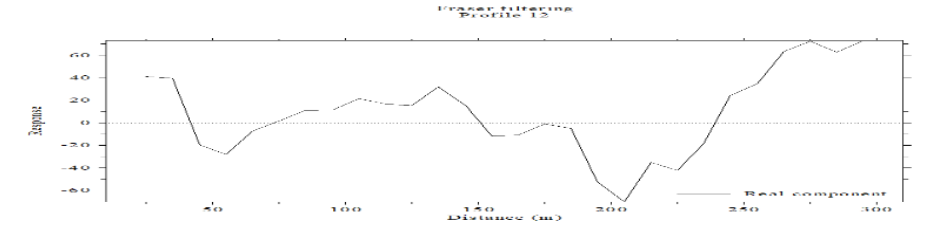


Figure 6: The VLF anomaly plot of in-phase fraser Filtered data and karouse-Hjelt Pseudo cross - section along traverse 2.



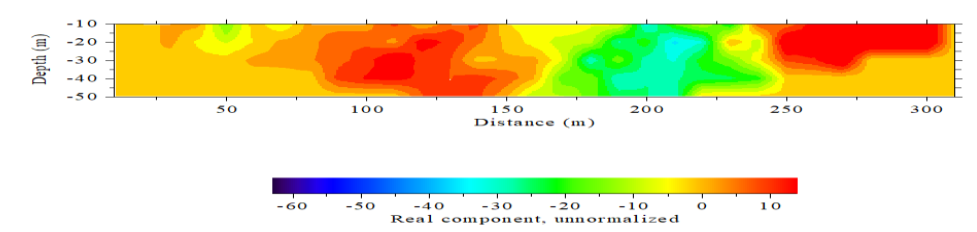


Figure 7: The VLF anomaly plot of in-phase fraser Filtered data and karouse-Hjelt Pseudo cross - section along traverse 3.

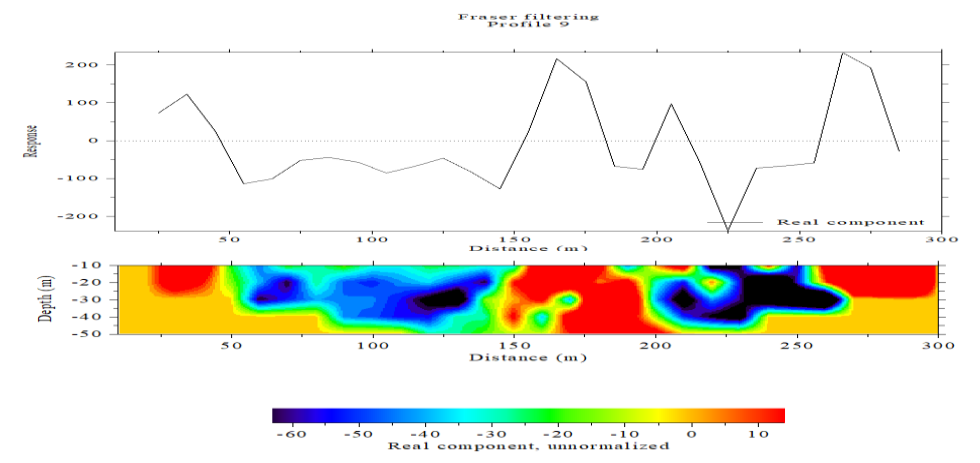


Figure 8: The VLF anomaly plot of in-phase fraser Filtered data and karouse-Hjelt Pseudo cross - section along traverse 4.

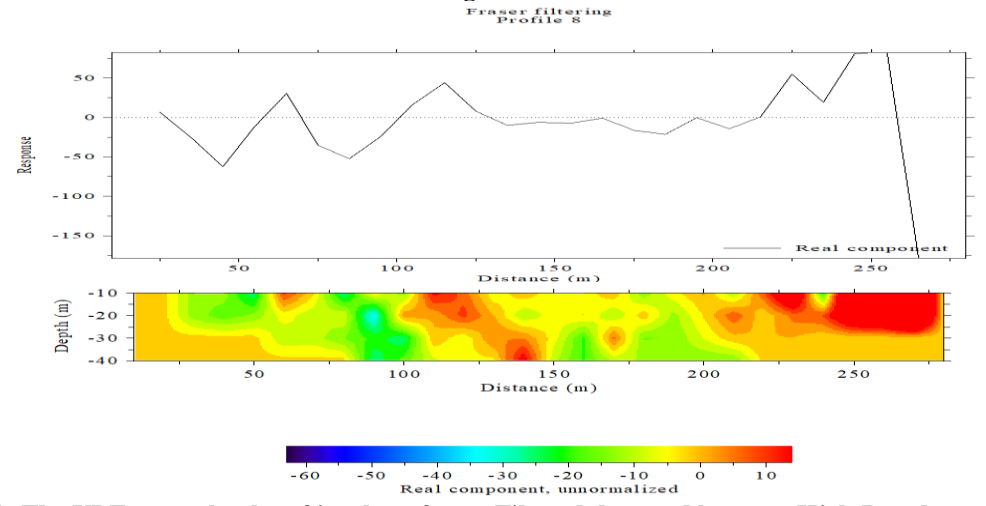
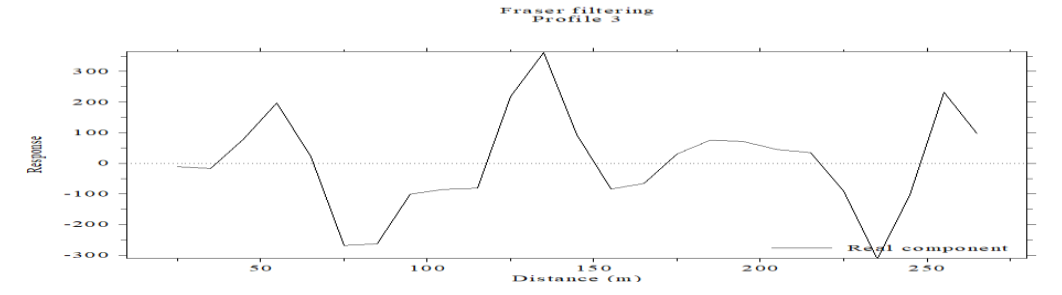


Figure 9: The VLF anomaly plot of in-phase fraser Filtered data and karouse-Hjelt Pseudo cross - section along traverse 5.



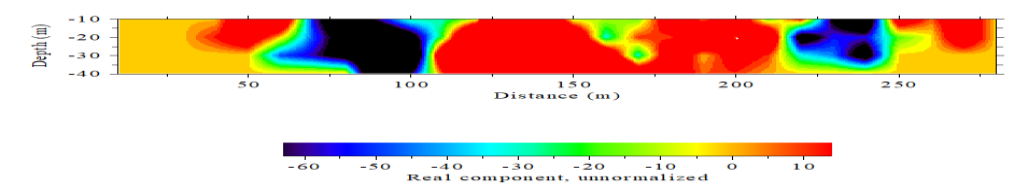


Figure 10: The VLF anomaly plot of in-phase fraser Filtered data and karouse-Hjelt Pseudo cross - section along traverse 6.

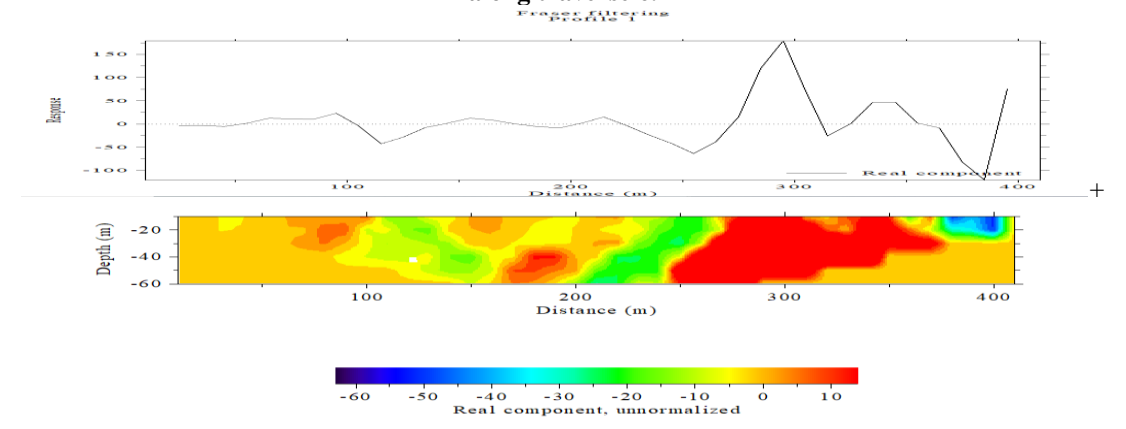


Figure 11: The VLF anomaly plot of in-phase fraser Filtered data and karouse-Hjelt Pseudo cross - section along traverse 7.

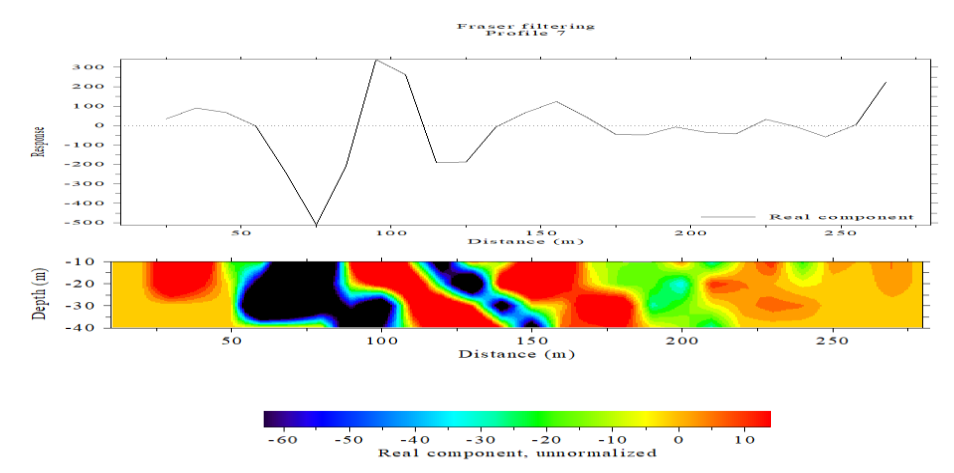
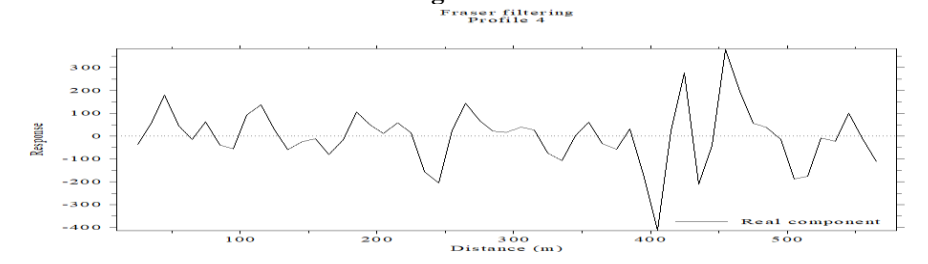


Figure 12: The VLF anomaly plot of in-phase fraser Filtered data and karouse-Hjelt Pseudo cross - section along traverse 8.



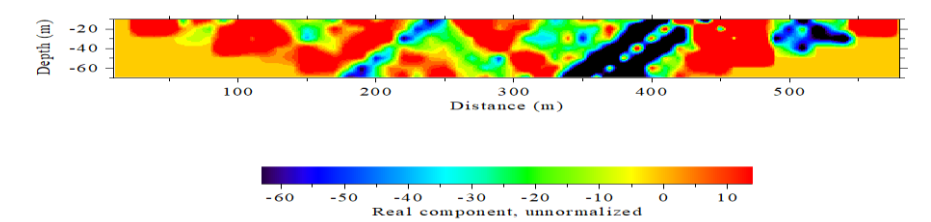


Figure 13: The VLF anomaly plot of in-phase fraser Filtered data and karouse-Hjelt Pseudo cross - section along traverse 9.

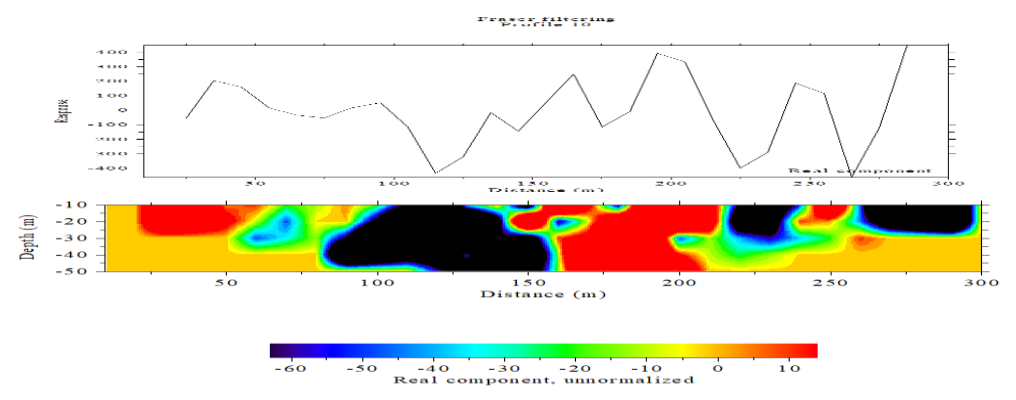


Figure 14: The VLF anomaly plot of in-phase fraser Filtered data and karouse-Hjelt Pseudo cross - section along traverse 10.

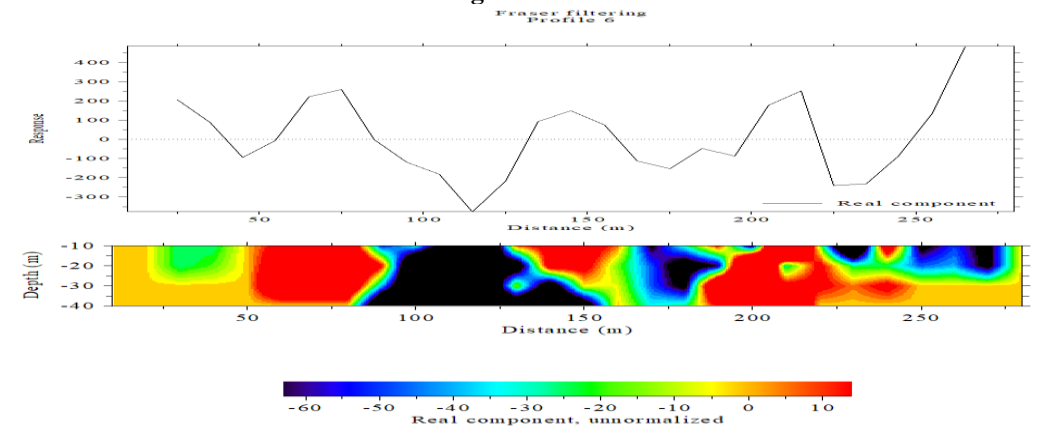
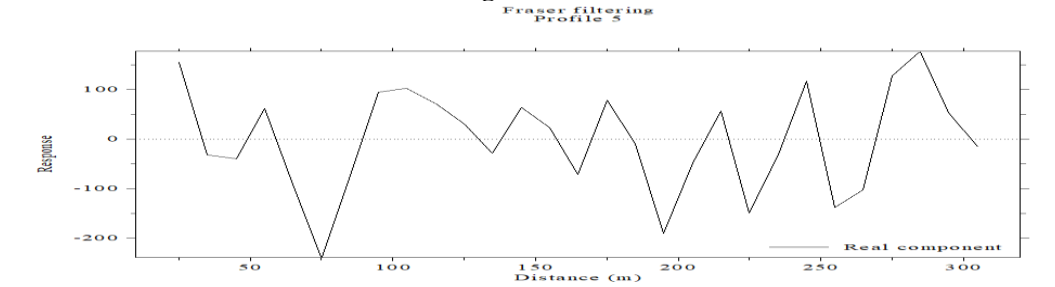


Figure 15: The VLF anomaly plot of in-phase fraser Filtered data and karouse-Hjelt Pseudo cross - section along traverse 11.



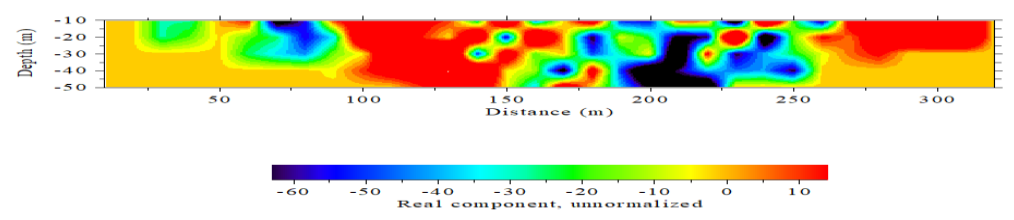


Figure 16: The VLF anomaly plot of in-phase fraser Filtered data and karouse-Hjelt Pseudo cross - section along traverse 12.

Discussions of the VLF-EM Results

Traverse 1 (Figure 5) is stretches from N-S at an approximately 500 m length. It shows three (3) major positive responses, the first which is more pronounced is situated between a distances of 140-250 m from the surface at a depth of 60 m. The second is between 240-300 m at a depth of 40 m from the surface. The last one is spotted at a distance of 260-340 m from the surface at a depth of 50 m very close to the second positive response with orientation at N-S and N-W respectively. These positive responses are indicative of possible fracture zones which indicate an aquifer zone and are good prospect for ground water.

Traverse 2 (**Figure 6**) shows significant anomalies which is an indication positive responses from a distance between 25-200 m at a depth of 50 m from the surface and a distance between 175-225 m at a depth 48 m respectively both occurring at deeper depthsoriented at N-E direction. There is no indication of a resistive body along the profile which makes it a good potential for groundwater accumulation interpreted as a faulted zone filled with fluids.

Two (2) aspects of positive responses are present in traverse 3 curves (Figure 7), ranging from 80-150 m at a depth of 50 m from the surface to 250-300 m at a depth of 40 moriented at N-E direction. There is a good chance that ground water will accumulate in these areas; hence the anomaly must have been caused by a fracture zone in the basement.

In Traverse 4 (Figure 8), three (3) positive responses were found and located at distances of 25–50 m, 150–200 m, and 250–300 m, respectively. At 30 m, 50 m, and 30 m depths, respectively oriented at N-E direction. These areas have good groundwater prospects and the anomaly must have been caused by a basement fracture zone that has a high potential for groundwater accumulation. The dry and compacted sand soil is probably the cause of the extremely resistant bodies that extend from the near surface to depths greater than 50 meters.

The line plot of traverse 5 is shown in Figure 9; it is 280 meters long overall and runs from north to south. a not well-fractured zone is located at a horizontal distance of between 0-150m, along the profile at depth of between 0-40m. The conductive zones are located at 100-150 m and 200-300 m respectively over the eastern portion of the profile all to depth of 40 m. the anomalyies are oriented in

N-E direction. In the filtered real map, these zones are clearly visible as peaks.

Travers 6 (Figure 10) is 280 meters long and orientated from north to south. As seen in figure 4.16, the filter yields three (3) main positive responses. The first is located at a depth of 28 meters and between 25 and 50 meters on the surface. The second is much more noticeable and dispersed across the middle of the profile; it is visible 40 meters below the surface and at distances of 120-210 meters. The third one, which is less noticeable, is located between 250 and 270 meters below the surface at a depth of 30 meters. The areas have good groundwater prospects. As can be observed, there are two primary regions with strong resistivity at 230-248 m and 60-105 m. These two extremely resistant zones extend from the surface to a rather shallow depth, as the apparent current density map demonstrates.

The length of **Figure 11**, extending from N to S, is 420 meters. With the first three located in the northern section at a distance of 60-10 m, 30 m below the surface, 140-175 m, 38 m below the surface, and 170-200 m, 40 m below the surface, the profile yields four (4) large positive responses. The fourth response occurs toward the southern part of the profile at a distance between 240-380m at 60m depth from the surface all oriented in N-E direction respectively. These zones are well displayed as peaks in the filtered real map which are indicative of possible fracture zones. The fourth response which is much more pronounced can be suggested for borehole drilling. Other areas on the apparent current density map indicate a highly resistive body suspected to be dry coarse-sandy material of high resistivity.

Three (3) conductive entities are also visible in the traverse 8 plots (Figure 12). The filtered real component shows a favorably peaked area. At a depth of 25 meters below the surface, the first positive response can be found between 25 and 50 meters. The second is seen 40 meters below the surface at a distance of 125 meters. The third one, which is 175 meters away, is thought to be a saturated zone inside the faulted or fractured basement. The anomalies in this profile are oriented in N-W direction.

The real and imaginary anomaly line-plot along traverse 9 is depicted in **Figure 13**. It demonstrates the existence of conductive zones at several large peaks,

which are located between 10 and 50 m, 80 and 140 m, 150 and 200 m, and 21 and 260 m, 250-330 m, 400-48 m and 550-600 m, respectively and the filtered real component map demonstrate these peaks. The highly resistive zones are also seen distances between 380-420 m and 490-550 m, respectively. This profile was taken along a tarred road the resulting anomaly is suspected to be as a result of noise from the Iron Gate and fencing as well as distribution lines along the profile.

The line-plot along traverse 10 in **Figure 14** demonstrates the presence of positive reactions zones at three (3) probable fracture zones with one highly conductive, the fractured zones are at corresponding distances of 25–50 m at a depth of 30 m, 150–210 m at a depth of 50 m for the high conductive zone, and 250 m at a depth of 20 m. These peaks are accentuated in the filtered real component map. The distances of the highly resistant zones are 75–160 m, 225 m, and 240–280 m, respectively. The highly resistive zones are understood as drycompacted sandy soils, whereas the favorable responses are interpreted as clayey/silty soil materials.

Figure 15 is the filtered data plot of traverse 11, it has a total length of 280 m and it is oriented in the N-S direction. The Fraser filtered gives three (3) major positive responses. The first is situated between a distances of 75-90 m at a depth of 40 m from the surface, The second is observed at a distance between of 125-160 m, at a depth of 25 m. The last one is spotted at a distance between 180-250 m at a depth of 40 m. These positive responses are indicative of possible fracture zones, these are potential aquifer and good prospect for ground water. The area around 180-160 m, 175 m and 225-275 m indicate a highly resistive body from near surface to depth 40 m, 39 m and 25 m respectively whichindicate the likely occurrence of dry consolidated soil.

Figure 16 is a plot oftraverse 12 demonstrate two significant anomaly which is an indication of two main conductive zones (fracture rock) around distances between 95-110 m and 260-420 m respectively with the first anomaly occurring at deeper depths while the second anomaly occurring at shallow depth. These two anomalies are zones of interest for groundwater extraction in the basement terrain. There is highly resistive zones between 60-90 m and 200-250 m extending to a depth 30 and 50 m as displayed in the anomaly, filtered real and the apparent current density map.

CONCLUSION

The VLF data successfully identified the real and imaginary curves which were used to delineate the conductive zones interpreted to be vertical basement fracturesor basement aquifer and possible areas of high groundwater accumulation. The VLF-EM data were acquired along twelve traverses. The results of the study suggest that the fractured zones were identified on all twelve traverses (Figures 5-12) which showed high

conductive zones indicative of fractured zones with a depth range of 0 to 60 m within the subsurface and are prominently oriented in the NE-SW and NW-SE direction. The study therefore recommends the drilling of productive and sustainable boreholes at locations traverse 1, traverse 2, traverse 4, traverse 6, traverse 7 and traverse 10 between 150-250 m, 75-175 m, 150-200 m, 120-220 m, 250-300 m and 160-220 m respectively along the profile. These aforementioned locations are prospective sites for further investigation for groundwater development in the study area.

We recommend additional detailed geophysical investigation using other complementary geophysical methods such asseismic refraction tomography capable of of detecting fractures in order to confirm the fracture zones delineated using the EM method and to elucidate the pattern of the fracture and also borehole validation and hydrogeochemical analysis alongside the complementary geophysics.

Acknowledgements

Many thanks to Nigeria geological Survey Agency (NGSA) for release of equipment used for the field work and theprovided expertise during the field work exercise. We are grateful to the Petroleum Technology Development Fund (PTDF) for the sponsorship

REFERENCES

Adiat, K.A. N., Adelusi, A.O. & Ayuk, M. A. (2009). Relevance of Geophysics in Road Failures Investigation in a Typical Basement Complex of Southwestern Nigeria. Geophysics, 29, 589-678.

Ayanninuola, O. S., Jatau, B. S. & Loko, A. Z. (2018) Geoelectric Soundings for the Determination of Aquifer Characteristics in Anjagwa, Nasarawa State Nigeria. Fuw Trends in Science & Technology Journal. 3 (2b): 938 – 943

Aisha, A. K., Abdulsamiu, M. I. & Ahmad, A. K. (2022). Hydrogeochemical Assessment of Groundwater around Gauta, Central Nigeria. Journal of Earth and Environmental Science Research. 4(2):1-8

Aisha, A. K. (2022). Heavy metal Assessment of Groundwater Quality in part of Karu, Central Nigeria. Water practice and technology. 17 (9): 1802-1817

Ahzegbobor, P. A. (2010). 2d And 3d Geoelectrical Resistivity Imaging: Theory and Field Design. Scientific Research and Essays Vol. 5(23), Pp. 3592-3605

Frohlich, R. K., & Kelly, W. E. (1985). The relation between hydraulic transmissivity and transverse resistance in a complicated aquifer of glacial outwash

deposits. Journal of Hydrology, 79, 215-219.

Fraser, D. C. (1969). Contouring of VLF-EM Data. Geophysics, 34, 958-967

Jatau, B.S., Yakubu, M. E., Tanko I.Y., Kana.A. I. & Ayanninuola, O.S. (2020). Assessment of Groundwater Potential of Risha Part of Akwanga Sheet 209ne, North Central Nigeria. International Research Journal of Natural Sciences. 8 (2): 1-15

Karous, M. R. & Hjelt, S. E. (1983). Linear filtering of VLF dip-angle measurement. Geophysical prospecting. 36, 782-894.

Kaikkonnen, P. and Sharma S.P. (1997): Delineation of near Surface Structures Using VLF and VLF-R Data aninsight From the Joint Inversion Result. *The Leading* Edge; 16(11), pp. 1683-1689

Nura, U. K., Mohammad, F. R., Ahmad, Z. A. & Wan-Nor, A. S. (2019). Hydraulic Parameters Estimation Using 2d Resistivity Technique: A Case Study in Kapas Island, Malaysia. Advances in Sustainable and Environmental Hydrology, Hydrogeology, Hydrochemistry and Water Resources, Advances In Science, Technology & Innovation. 4(3): 245-248

Saaty, T. L. (1980). The Analytic Hierarchy Process. McGraw-Hill. (Canonical reference for AHP and pairwise weight derivation in MCDA).

Singha, A.K. (1990): Interpretation of Ground VLF-EM data In terms of Inclined Sheet-Like Conductor Model PAGEOPH; 132(4), pp. 733–755